Title

Functional stabilization of weakened thalamic pacemaker channel regulation in rat absence epilepsy.

Journal

The Journal of physiology, 575(Pt 1)

ISSN

0022-3751

Authors

Kuisle, Mira
Wanaverbecq, Nicolas
Brewster, Amy L
et al.

Publication Date

2006-08-01

DOI

10.1113/jphysiol.2006.110486

Functional stabilization of weakened thalamic pacemaker channel regulation in rat absence epilepsy

Mira Kuisle[1], Nicolas Wanaverbecq[1], Amy L. Brewster[2], Samuel G. A. Frère[1], Didier Pinault[3], Tallie Z. Baram[2] and Anita Lüthi[1]

[1] *Department of Pharmacology and Neurobiology, Biozentrum, Klingelbergstr. 70, CH-4056 Basel, Switzerland*
[2] *Departments of Anatomy/Neurobiology and Pediatrics, University of California at Irvine, Irvine, CA 92697, USA*
[3] *INSERM U666, Physiopathologie clinique et expérimentale de la schizophrénie, Faculté de Médecine, 11 rue Humann, F-67085, Strasbourg, France*

Aberrant function of pacemaker currents (I_h), carried by hyperpolarization-activated cation non-selective (HCN) channels, affects neuronal excitability and accompanies epilepsy, but its distinct roles in epileptogenesis and chronic epilepsy are unclear. We probed I_h function and subunit composition during both pre- and chronically epileptic stages in thalamocortical (TC) neurones of the Genetic Absence Epilepsy Rat from Strasbourg (GAERS). Voltage gating of I_h was unaltered in mature somatosensory TC cells, both *in vivo* and *in vitro*. However, the enhancement of I_h by phasic, near-physiological, cAMP pulses was diminished by ∼40% and the half-maximal cAMP concentration increased by ∼5-fold. This decreased responsiveness of I_h to its major cellular modulator preceded epilepsy onset in GAERS, persisted throughout the chronic state, and was accompanied by an enhanced expression of the cAMP-insensitive HCN1 channel mRNA (> 50%), without changes in the mRNA levels of HCN2 and HCN4. To assess for alterations in TC cell excitability, we monitored the slow up-regulation of I_h that is induced by Ca^{2+}-triggered cAMP synthesis and important for terminating *in vitro* synchronized oscillations. Remarkably, repetitive rebound Ca^{2+} spikes evoked normal slow I_h up-regulation in mature GAERS neurones; that sufficed to attenuate spontaneous rhythmic burst discharges. These adaptive mechanisms occurred upstream of cAMP turnover and involved enhanced intracellular Ca^{2+} accumulation upon repetitive low-threshold Ca^{2+} discharges. Therefore, HCN channels appear to play a dual role in epilepsy. Weakened cAMP binding to HCN channels precedes, and likely promotes, epileptogenesis in GAERS, whereas compensatory mechanisms stabilizing I_h function contribute to the termination of spike-and-wave discharges in chronic epilepsy.

(Resubmitted 5 April 2006; accepted after revision 23 May 2006; first published online 25 May 2006)
Corresponding author A. Lüthi: Department of Pharmacology and Neurobiology, Klingelbergstr. 70, CH-4056 Basel, Switzerland. Email: anita.luthi@unibas.ch

The hyperpolarization-activated cation non-selective (HCN) channels are emerging as important targets in neurological diseases, including epilepsy (Santoro & Baram, 2003; Bender *et al.* 2004; Frère *et al.* 2004; Poolos, 2004). HCN channels give rise to hyperpolarization-activated inward currents (I_h) that are sensitive to intracellular cAMP levels (Pape, 1996; Robinson & Siegelbaum, 2003). The dual gating by voltage and cAMP allows I_h to widely control neuronal and network excitability (Santoro & Baram, 2003; Frère *et al.* 2004). Furthermore, I_h is regulated by neuronal activity, including seizures: hippocampal I_h is acutely increased by synaptically released glutamate (van Welie *et al.* 2004), and abnormal regulation of I_h and of HCN channel subunit expression occurs in brain regions involved in seizure generation (Di Pasquale *et al.* 1997; Chen *et al.* 2001*a*; Brewster *et al.* 2002; Bender *et al.* 2003; Shah *et al.* 2004; Strauss *et al.* 2004; Budde *et al.* 2005), suggesting that modified HCN channel function may contribute to hyperexcitability.

The recognition of an involvement of I_h in epileptic processes has prompted much interest into how aberrant I_h function is causally linked to the initiation and the maintenance of seizures. Both inherited deficits in HCN channel function, present before epilepsy onset, and acquired modifications resulting from seizure activity, could contribute to the epileptic phenotype. However, the role of I_h in epilepsy was mostly studied in either

M. Kuisle, N. Wanaverbecq and A. L. Brewster contributed equally to this work.

DOI: 10.1113/jphysiol.2006.110486

pre-epileptic (Shah *et al.* 2004; Budde *et al.* 2005) or chronic epileptic conditions (Chen *et al.* 2001*a*; Strauss *et al.* 2004), leaving the relative importance of inherited and acquired channel alterations undetermined (Poolos, 2004). Furthermore, epileptic models showing perturbations in I_h are often accompanied by additional changes in ion channel or synaptic function (Tsakiridou *et al.* 1995; Di Pasquale *et al.* 1997; Chen *et al.* 2001*a*; Zhang *et al.* 2002; Klein *et al.* 2004; Holter *et al.* 2005), thereby modifying I_h-dependent changes in excitability. Finally, HCN channel subunit composition strongly determines the gating by cAMP (Chen *et al.* 2001*b*; Altomare *et al.* 2003; Budde *et al.* 2005), but whether altered isoform expression affects the efficacy of cAMP transients produced during neuronal activity is not clear.

Abnormal expression and regulation of HCN channels in thalamus and cortex was found in rodent models of generalized absence epilepsy, recognized by spike-and-wave discharges (SWDs) in the EEG (Di Pasquale *et al.* 1997; Strauss *et al.* 2004; Budde *et al.* 2005). A principal way by which HCN-channel-mediated currents may be gated during SWDs is via a transient cAMP synthesis that is triggered, to a large extent, by Ca^{2+} entry through the low-threshold (LT) Ca^{2+} spikes (Lüthi & McCormick, 1999*b*; Wang *et al.* 2002). The resulting slow afterdepolarization (ADP) terminates synchronized thalamic oscillations *in vitro* (Bal & McCormick, 1996; Lüthi *et al.* 1998). Here, we identified a diminished cAMP-dependent I_h regulation that was apparent before seizure onset in thalamocortical (TC) cells of the Genetic Absence Epilepsy Rat from Strasbourg (GAERS), a well-recognized genetic model of absence epilepsy, and persisted throughout the chronic epileptic state. However, adaptive mechanisms upstream of cAMP turnover, involving enhanced intracellular Ca^{2+} accumulation during repetitive LT Ca^{2+} spiking, restored the activity-dependent current up-regulation in mature TC cells, thereby contributing to the termination of SWDs.

Methods

All experiments were performed according to the guidelines of the institutions and the Veterinary Offices (Comité Régional d'Ethique en Matière d'Expérimentation Animale, Strasbourg, France; Veterinäramt Basel-Stadt, Switzerland; UCI Animal Care committee), and conformed to NIH guidelines.

In vivo electrophysiological recordings

Experiments were conducted in inbred, adult male Wistar rats (71 GAERS and 56 control non-epileptic (NE) rats, 3–6 months). All surgical procedures were made under deep general anaesthesia (pentobarbital: 40 mg kg^{-1}, I.P., and ketamine: 50 mg kg^{-1}, I.M.). A tracheotomy and a catheterization of the penile vein were performed, and the animal was placed in a stereotaxic frame (David Kopf Instruments, Tujunga, CA, USA). A stabilizing craniotomy–duratomy technique was systematically applied to improve the success rate of single-cell electrophysiology experiments, to increase the precision to reach stereotaxically single neurons in a target region, and to eliminate undesirable non-neuronal rhythms (heart and respiratory movements) during intracellular recordings (Pinault, 2005). The rat's rectal temperature was maintained at 37°C with a thermo-regulated blanket (Fine Science Tools, Heidelberg, Germany).

The neuroleptanalgesia was initiated before the end of the general pentobarbital–ketamine anaesthesia, then maintained by an intravenous injection of a mixture containing D-tubocurarine chloride, fentanyl, haldol and glucose (Pinault, 2003). All rats were artificially ventilated in the pressure mode (SAR-830, CWE, Ardmore, PA; 8–12 cmH_2O; 60–65 breaths min^{-1}) using an O_2-enriched gas mixture (70–50% air, 30–50% O_2). The EEG, which displayed spontaneously synchronized slow oscillations (Pinault, 2003), and heart rate were also continuously monitored to maintain a constant depth of anaesthesia by adjusting the injection rate of the anaesthetic solution. Subcutaneous infiltrations of xylocaine (2%) were applied every 3 h at all surgical sites.

Glass micropipettes (30–70 MΩ) were filled with a solution containing 1.5% *N*-(2-aminoethyl)biotinamide hydrochloride (Neurobiotin) dissolved in 1 M potassium acetate. It was then lowered with a stepping microdriver (Burleigh, Fishers, NY, USA) into the somatosensory thalamus to reach a single TC neurone (Fig. 1*A*), which was extracellularly and/or intracellularly recorded simultaneously with the EEG of the frontoparietal cortex.

Electrophysiological data were processed with band passes of 0.1–1200 Hz for the EEG, and of 0–6 kHz for cellular activity (Cyber-Amp 380, Molecular Devices, Union City, CA, USA). Signals were digitized at a sampling rate > 18 kHz. During the intracellular recording session, a current pulse in the range from −0.2 to −0.5 nA was applied every 2 s to keep the Wheatstone bridge balanced. Using square wave current pulses (range of ± 3 nA), input membrane resistance and intrinsic firing patterns of thalamic neurones could be assessed.

At the end of the recording session, some of the units were individually labelled using the intracellular tracer microiontophoresis technique for standard histological identification (Fig. 1*Ab*). After a survival time of at least 30 min, animals were killed with an intravenous overdose of pentobarbital, transcardially perfused with 4% paraformaldehyde and 0.25% glutaraldehyde in 10 mM phosphate-buffered saline, and the brain tissue

was processed using standard histological techniques for retrieving the tracer-filled neurones.

Electrophysiological recordings were analysed with the pCLAMP 7.01 software (Molecular Devices), and the tracer-filled neurones were examined with a light microscope (E600, Nikon, Champigny-sur-Marne, France). Some of the neurones were reconstructed using the Neurolucida system (Microbrigthfield, Colchester, VT, USA) (Fig. 1*Ac*). The location of marked cells was ascertained by consulting a stereotaxic atlas (Paxinos & Watson, 1998).

In vitro electrophysiological recordings

Slices were prepared from mature, chronically epileptic rats (3–8 months) or young pre-epileptic animals (19–24 days) and age-matched NE control animals. The majority of the experiments were carried out blind to the colony from which the animals were derived. Rats were deeply anaesthetized with isoflurane vapour in a mobile anaesthesia station (Provet, Switzerland) and immediately decapitated. Coronal slices (300 μm) containing the somatosensory ventrobasal nuclear complex were prepared on a vibratome (VT1000S, Leica, Glattbrugg, Switzerland) in an ice-cold oxygenated solution containing (mM): 63 NaCl, 107 sucrose, 2.5 KCl, 1.25 NaH_2PO_4, 26 $NaHCO_3$, 0.5 $CaCl_2$, 7 $MgCl_2$, 18 dextrose, 1.7 L(+)-ascorbic acid. The slices were allowed to recover for 5 min in a home-made interface-type chamber at 35.0°C in the cutting solution, before being transferred to a sucrose-free solution containing 126 mM NaCl instead, and cation concentrations were altered to 2 mM $CaCl_2$ and 4 mM $MgCl_2$. After an additional 30 min, slices were incubated at room temperature for 1–2 h and then transferred individually into the recording chamber. Pretreatment of slices with the adenylyl cyclase inhibitor SQ22,536 started ~30 min after incubation at room temperature. Slices were transferred for at least 2 h to a small interface chamber containing 10 ml of 0.6 mM SQ22,536 before recordings commenced in SQ22,536-free bathing solution. SQ22,536-treated slices were used for maximally 1 h in the recording chamber.

Whole-cell recordings were obtained from TC neurones under visual control using differential interference contrast microscopy via upright microscopes (Olympus BX50WI and BX51WI, Volketswil, Switzerland) at 33.5–35°C. The location of the ventroposterior medial nucleus (Vpm) of the somatosensory thalamus was determined before pipette positioning using a 10 × objective, and was clearly recognizable based on its apposition to the ventroposterior lateral nucleus (Vpl), which has a striated appearance. Slices were not used when the Vpm could not be clearly delineated. Patch pipettes were pulled from borosilicate glass tubing (TW150F-4, outer diameter 1.5 mm, WPI, Berlin, Germany) on a vertical two-step puller (PP-83, Narishige, Tokyo, Japan) and filled with the following solution (mM): 130 potassium gluconate, 10 KCl, 10 Hepes, 2 $MgCl_2$, 2 Na_2ATP, 0.2 NaGTP, 10 phosphocreatine, adjusted to 290 mosmol l^{-1} with sucrose, pH 7.25. This solution was found previously to yield ADPs with kinetics and amplitudes similar to those reported from microelectrode recordings (Bal & McCormick, 1996), indicating that it minimally perturbed the cytosolic components required for the generation of the ADP. GTP was freshly added daily from stocks (100-fold concentrated). The resistance of the electrodes was 2.5–4 MΩ and yielded series resistances in the range between 7 and 19 MΩ. If series resistance changed by more than 10%, the experiment was not included in the analysis. A liquid junction potential of 10 mV measured as described (Neher, 1992) was taken into account for all data. The bath was constantly perfused with fresh medium at a rate of 3 ml min^{-1} throughout the recording and contained (mM): 126 NaCl; 2.5 KCl; 1.25 NaH_2PO_4; 2 $MgCl_2$; 2 $CaCl_2$; 26 $NaHCO_3$, 18 dextrose, 1.7 L(+)-ascorbic acid. Data from voltage- and current-clamp recordings were collected through an Axopatch 200B amplifier (Molecular Devices), filtered at 2 kHz and acquired at 5 kHz using pCLAMP 9.2. software. Slices preincubated with SQ22,536 showed an attenuated amplitude of the ADP (2.5 ± 0.4 mV in control, $n = 6$, 1.4 ± 0.2 mV in SQ22,536, $n = 4$, $P < 0.05$), indicating that stimulation of adenylyl cyclases was selectively reduced, but a hyperpolarization-induced sag potential was unchanged, reflecting unaffected voltage gating of I_h around −80 mV (5.8 ± 0.3 mV, $n = 45$ in control, 6.0 ± 0.3 mV, $n = 77$ in SQ22,536, $P > 0.05$). For the data included in the 8Br-cAMP concentration–response curve (Fig. 2*G*), the average series resistances did not differ between the groups (12.0 ± 0.4 MΩ, $n = 32$, and 11.5 ± 0.3 MΩ, $n = 31$, for cells derived from NE animals and GAERS, respectively, $P > 0.05$). Tail current analysis was applied for determining activation curves of I_h. Igor v. 4.0.8 (WaveMetrics, Inc., Lake Oswego, OR, USA) was used for fitting Boltzman and Hill equations to I_h activation curves and 8Br-cAMP concentration–response curves, respectively. Hill coefficients were fixed at values between 1 and 1.4 (Lüthi & McCormick, 1999*b*; Chen *et al.* 2001*b*), yielding half-maximal concentrations that differed by < 5%.

The values for $V_{1/2}$ were derived from the average of one to four activation curves obtained within a recording time of 5–20 min after gaining whole-cell access. Caged cAMP (P^1-2-nitrophenyl)ethylester, 100 μM) was added to the patch solution from a 100-fold concentrated stock solution in DMSO immediately before the experiment and the pipette solution was kept on ice and protected from light. A minimal time of ~3–5 min was allowed for the perfusion of caged cAMP and 8Br-cAMP (0.1–10 μM)

into the cell. Flashes were applied with a ultraviolet (UV) lamp attached to the epifluorescence pathway of the microscope and discharged via the capacitive discharges of the FlashMic (80% of maximal capacitive charge, Rapp Optoelectronics, Hamburg, Germany). This procedure permits the generation of cAMP transients in a reproducible manner and was previously used to establish dose–response curves (Lüthi & McCormick, 1999*b*). Current amplitudes were measured with 1.5 s voltage steps from −60 to −90 mV at 4 s intervals and quantified by averaging responses of two successive flashes applied at intervals > 1 min. Amplitudes of ADPs were quantified 2 s after termination of the last current injection. Amplitudes of currents and ADPs were measured in Clampfit (v. 9.0; Molecular Devices).

Quantitative *in situ* hybridization and Western blotting

For *in situ* hybridization procedures, rats were killed with an overdose of pentobarbital (250 mg kg^{-1}, I.P.) and quickly decapitated (4–5 rats per group), brains dissected and placed on powdered dry ice. Quantitative analyses of thalamic HCN isoform mRNA levels were accomplished using antisense ^{35}S-cRNA probes synthetized by *in vitro* transcription from cDNAs containing specific gene regions of mouse HCN1, HCN2 and HCN4 channels (Brewster *et al.* 2002; Bender *et al.* 2003). Briefly, 20 μm-thick brain sections were cut, mounted on gel-coated slides and fixed in 4% paraformaldehyde. Following a graded ethanol treatment, sections were exposed to acetic anhydride-triethanolamine, then dehydrated through 70–100% ethanol. Sections were then preincubated in hybridization solution (50% formamide, 5× SET, 0.2% sodium dodecyl sulphate, 5× Denhardt's solution, 0.5 mg ml^{-1} salmon sperm sheared DNA, 250 g l^{-1} yeast tRNA, 100 mM DTT, 10% dextran sulphate) and probed overnight at 55°C with antisense ^{35}S-CTP radiolabelled HCN probes (0.5–1 × 10^6 c.p.m. (30 μl)$^{-1}$ per section). The specific activity of the probes was 1.67–5.2 × 10^8 c.p.m. μg^{-1}. On the following day, sections were washed in decreasing concentrations of saline sodium citrate (SSC) solutions, with the most stringent wash at 0.03 × SSC for 60 min at 62°C. Following dehydration in increasing alcohol concentrations, sections were apposed against Kodak Biomax films. Optimal exposure time was monitored using ^{14}C standards to maintain signal linearity.

All analyses were performed by investigators unaware of the origin (GAERS *versus* NE animals) of all samples. Data acquisition and quantification of *in situ* hybridization signals were carried out on sections run concurrently by measuring optical density (OD) of incorporated radioactivity in Vpm and Rtn using the image analysis program ImageTool (v. 1.25; University of Texas Health Science Center, San Antonio, TX, USA) (Brewster *et al.* 2002). The OD measured over the corpus callosum was used as background signal. Linearity of hybridization signal was ascertained using ^{14}C standards (American Radiolabelled Chemicals Inc., St Louis, MO, USA). Statistical analyses for *in situ* hybridization data were performed using Prism software (GraphPad Software Inc., San Diego, CA, USA).

Western blots were performed as previously described (Brewster *et al.* 2005, 2006). Briefly, each sample consisted of a whole thalamic extract from an individual rat. Dissected tissue was immediately frozen in dry ice and then homogenized in glass/Teflon homogenizers in ice-cold 0.32 M sucrose, 0.1 M Tris-HCl (pH 7.4)-containing Protease Inhibitor Cocktail (PIC Complete^{TM} Anaesthetics, chemicals and reagents; diluted according to manufacturer's instructions). Samples were centrifuged at 1000 *g* for 10 min at 4°C and the pellet was discarded. The resulting supernatant was centrifuged at 16 000 *g* for 20 min at 4°C and the pellet containing membrane fractions resuspended in ACSF (124 mM NaCl, 3 mM KCl, 1.25 mM KH_2PO_4, 2.5 mM $MgSO_4$, 3.4 mM $CaCl_2$, 26 mM $NaHCO_3$, 10 mM glucose, 1× PIC). Protein concentration was determined using the Bio-Rad protein assay (Bio-Rad, Hercules, CA, USA). Equal amounts of protein were diluted in Laemmli buffer, separated by SDS-PAGE and visualized using the enhanced chemiluminescence ECL-Plus kit (Amersham Pharmacia Biotech; Piscataway, NJ, USA) as previously described (Brewster *et al.* 2005, 2006). Briefly, 30 μg of protein extracts was separated with 4–12% SDS-PAGE and transferred to Hybond-P polyvinyl difluoride membranes (Amersham Pharmacia). Membranes were blocked with 10% non-fat milk in PBS overnight at 4°C and were probed with rabbit anti-HCN1, rabbit anti-HCN2 (1 : 500 each) or rabbit anti-actin antisera (1 : 40 000) overnight at 4°C. Following washes in PBS–1% Tween (PBS-T) (3 × 5 min), membranes were incubated with secondary antibodies in PBS for 1 h at room temperature. Membranes were then washed in PBS-T (3 × 5 min) and incubated with ECL-Plus. Immunoreactive bands were visualized by apposing membranes to Hyperfilm ECL (Amersham Pharmacia).

Fluorescence imaging of intracellular Ca^{2+} concentrations

Relative fluorescence changes ($\Delta F/F$) of the long-wavelength Ca^{2+} indicator Oregon Green 488 BAPTA-2 (75 μM; $K_d = 580$ nM) were used to compare intracellular Ca^{2+} levels reached after single or repetitive rebound Ca^{2+} spikes (up to 16 pulses, 4 Hz, −0.9 nA current injection for 125 ms) in adult NE animals and GAERS (4–8 months). The dye was added to the intracellular solution (see above) and the cells were perfused via the patch pipette for 10–25 min, until proximal dendrites of TC cells could be visualized. Intracellular perfusion with the dye did

not alter resting membrane potentials (-62.9 ± 0.7 mV, $n = 10$ and -62.0 ± 1.1 mV, $n = 7$, for NE and GAERS cells, respectively, $P > 0.05$) nor amplitudes of evoked ADPs (2.1 ± 0.2 mV, $n = 10$, and 2.3 ± 0.4 mV, $n = 7$ for NE and GAERS cells, respectively, $P > 0.05$). Excitation occurred at 488 nm using a Polychrome IV (TILL Photonics, Gräfelfing, Germany), and the light emitted at 510 nm was collected via a cooled CCD camera (Imago VGA, 480 pixels × 640 pixels) after passing through a 40× objective and an Olympus fluorescein isothiocyanate filter set. Images were acquired for 150 ms using a binning of 8 at 0.2 s intervals during and at 0.5 s intervals before and after stimulation. The image acquisition was synchronized with the electrophysiological recordings using the Sync output of the imaging control unit, and data were analysed using Till Vision Imaging Software (v. 4.01) and SigmaPlot (v. 8.0) for fitting the time course of decay. Average fluorescence was determined for regions of interest (typically 80–400 μm^2) over the soma (avoiding the nucleus) or a stem dendrite, and the average background fluorescence of a region away from the filled cell, with the threshold fluorescence level set to 10, was subtracted. Relative fluorescence ($\Delta F/F$ as a percentage) was calculated for each image: ((Average fluorescence − Average baseline fluorescence) × 100/Average baseline fluorescence). Baseline fluorescence was determined by the average of seven images before application of repetitive current injections. Ca^{2+} signals elicited by the protocols used for evoking ADPs were obtained at periods of 25 s and five successive sweeps were averaged in each cell. Minimal photobleaching was observed and the fluorescence change for each individual sweep was calculated with respect to the baseline signal prior to cell stimulation.

Anaesthetics, chemicals and reagents

Pentobarbital was purchased from Sanofi, Libourne, France, and ketamine from Merial, Lyon, France. Fentanyl and haldol were obtained from Janssen, Boulogne-Billancourt, France; xylocaine from Astra, Rueil-Malmaison, France; Neurobiotin was from Vector Laboratories, Burlingame, CA, USA. Caged cAMP was obtained from Calbiochem and Oregon Green 488 BAPTA-2 from Molecular Probes. Rabbit anti-HCN1 and anti-HCN2 antibodies were obtained from Chemicon, Temecula, CA, USA. PIC Complete was purchased from Roche, Alameda, CA, USA. d-Tubocurarine chloride, salts and chemicals, and rabbit anti-actin antisera were purchased from Sigma-Aldrich.

Statistical analysis

Data were evaluated for statistical significance using paired or unpaired Student's *t* test and ANOVA as appropriate, unless otherwise indicated. Significance level was set to 0.05. Data are presented as means ± S.E.M.

Results

Unaltered hyperpolarization-activated depolarizing sag potentials in TC neurones in adult GAERS *in vivo*

The h-current functions as a pacemaker for thalamic neuronal and network oscillations, and alterations in its voltage dependence strongly affect the propensity of TC cells to generate oscillatory burst discharges (Pape, 1996; Lüthi & McCormick, 1998*a*). To determine whether voltage gating of I_h was affected in GAERS, intracellular recordings were performed *in vivo* from 73 and 61 TC neurones in GAERS and NE animals, respectively. The data reported here are based, respectively, on 55 and 45 recordings, which fulfilled the following three criteria: (1) a stable resting membrane potential without holding polarizing current; (2) a firing pattern similar to that recorded extracellularly in the same or in other TC neurones; and (3) an overshooting of the action potentials. The recordings were performed in the Vpl and Vpm nuclei, the nuclei known to be primarily involved in SWDs in GAERS (Vergnes *et al.* 1990; Seidenbecher *et al.* 1998; Manning *et al.* 2004). The location of recorded neurones was ascertained on the basis of their stereotaxic location, their receptive field, and/or their labelling (Fig. 1*A*). Impaled neurones were assessed for resting membrane potential, input resistance, and a depolarizing sag potential, the physiological correlate of I_h voltage gating (Table 1). No significant differences in passive and active membrane properties were found between TC neurones of Vpl and Vpm nuclei. Two principal types of TC neurones were distinguished based on their ability to generate a measurable depolarizing sag potential (maximal sag amplitude ≥ 1 mV at a membrane potential < −75 mV) (Fig. 1*B*). The proportion of sag-displaying TC neurones ('sag cells') recorded in GAERS and NE rats was comparable (76.4% *versus* 62.2%, $\chi^2 = 2.357$, d.f. = 1, not significant (NS)). Moreover, in both GAERS and NE rats, the amplitude of the sag increased similarly as a function of membrane polarization, with values reaching 1.3 ± 0.2 mV and 1.5 ± 0.3 mV with V_{jump} between −65 and −70 mV, 2.6 ± 0.5 mV and 3.2 ± 0.6 mV between −75 and −80 mV, and 9.9 ± 1.5 mV and 9.1 ± 0.8 mV between −95 and −100 mV for NE ($n = 22$) and GAERS ($n = 28$) cells, respectively (NS; Fig. 1*C* and *D*). Neurones generating sags had, on average, a higher input resistance than neurones without a sag ('non-sag cells') and a more depolarized mean resting membrane potential (Table 1). Taken together, the fraction of I_h-expressing cells and the sag amplitudes were unaffected in the epileptic rat strain.

Reduced sensitivity of I_h to near-physiological cAMP pulses in both pre-epileptic and mature GAERS

The voltage dependence of I_h is regulated by cAMP, and the high cAMP sensitivity of thalamic I_h is essential for its multiple roles in thalamic oscillatory behaviour (Lüthi & McCormick, 1998*a*). Therefore, we next investigated cAMP-dependent modulation of I_h in whole-cell patch-clamp recordings in thalamic slice preparations *in vitro* from adult NE rats and GAERS. Slices used for these experiments were pretreated with SQ22,536 (0.6 mM), an adenylyl cyclase inhibitor, to minimize binding of endogenous cAMP to the channels (see Methods). Values of basic cellular properties and the quality of electrical access during recordings were similar for both strains (resting membrane potential -59.0 ± 3.0 mV for NE, $n = 8$, -60.4 ± 1.6 mV for GAERS, $n = 7$, NS; input resistance 223 ± 56 MΩ for NE, $n = 8$, 156 ± 27 MΩ for GAERS, $n = 7$, NS; series resistance 11.8 ± 0.6 MΩ for NE, $n = 8$, 12.0 ± 0.9 MΩ for GAERS, $n = 7$, NS). To probe the sensitivity of I_h to cAMP in mature NE rats and GAERS, we initially bath-applied the non-hydrolysable analogue of cAMP, 8Br-cAMP (1 mM), to TC cells located in the Vpm (Fig. 2*A* and *B*). Gradual wash-in of 8Br-cAMP (1 mM) enhanced current amplitude at -90 mV by a similar extent; from

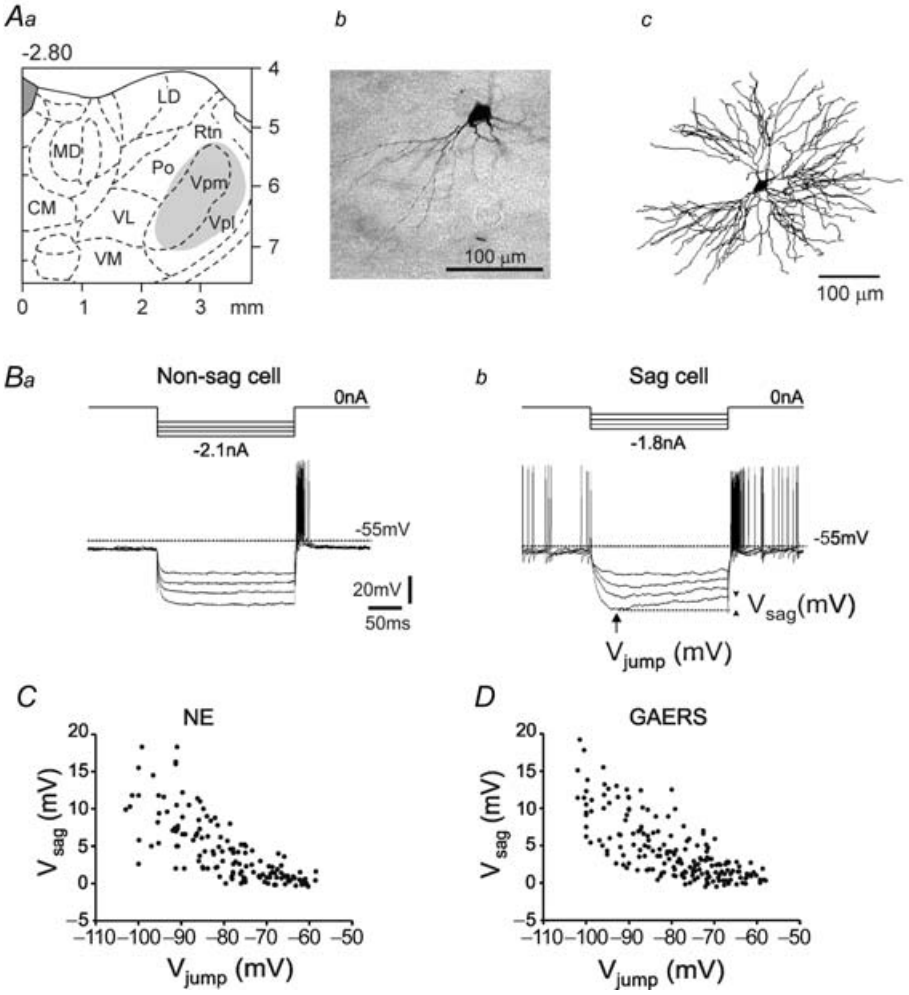

Figure 1. Hyperpolarization-induced depolarizing sags in thalamocortical (TC) neurones *in vivo*
Aa, stereotaxic location (2.8 ± 0.2 mm posterior to bregma) of the intracellularly recorded TC neurones (grey *area*). *Ab* and *c*, photomicrograph and 3D reconstruction of a typical TC neurone intracellularly labelled with Neurobiotin in the Vpm nucleus (frontal section). *Ba* and *b*, four voltage responses to 200 ms hyperpolarizing current pulses of increasing intensity in a neurone without (left, 'non-sag cell') and with (right, 'sag cell') a sag. The sag amplitude (V_{sag}) was measured as indicated in *Bb* (arrowheads). *C* and *D*, plot of V_{sag} amplitudes *versus* V_{jump} values in TC neurones of GAERS (*C*; $n = 28$ cells with at least 5 values per cell) and of control non-epileptic (NE) rats (*D*; $n = 22$ cells with at least 5 values per cell). CM = central medial; LD = lateral dorsal; MD = medial dorsal; Po = posterior thalamic nuclear group; VL = ventral lateral; VM = ventral medial; Vpl = ventral posterolateral; Vpm = ventral posteromedial; Rtn = nucleus reticularis thalami.

-370 ± 40 pA to -463 ± 36 pA ($n = 8$, $P < 0.001$) in NE, and from -329 ± 47 pA to -462 ± 58 pA in GAERS ($n = 7$, $P < 0.025$; Fig. 2*C*). Half-activation voltages ($V_{1/2}$) shifted from -89.6 ± 0.6 mV to -81.5 ± 0.9 mV ($n = 7$, $P < 0.001$; Fig. 2*B* and *C*) in GAERS, with the slope values remaining unchanged (from 8.5 ± 0.7 mV to 9.7 ± 0.7 mV, NS). Cells from mature NE rats yielded a shift from -87.5 ± 0.9 mV to -78.6 ± 1.6 mV ($n = 8$, $P < 0.001$; Fig. 2*A* and *C*) and the slope values were 8.3 ± 0.5 mV and 9.2 ± 0.8 mV (NS compared to corresponding values from GAERS), respectively. Therefore, when exposed to high steady levels of 8Br-cAMP, the sensitivity of thalamic I_h to the cyclic nucleotide is indistinguishable between GAERS and NE animals.

We next sought to investigate whether I_h in GAERS and NE animals differed in cAMP sensitivity during cAMP signals approximating physiological situations. Indeed, activity-dependent alterations in cAMP levels occurring during spontaneous thalamic oscillations *in vitro* are phasic and only partially shift the voltage dependence of I_h (Lüthi & McCormick, 1998*b*). We found previously that, by using photolytic release of cAMP, we induced a dose-dependent, submaximal enhancement of I_h, which is occluded by Ca^{2+}-dependent I_h up-regulation (Lüthi & McCormick, 1999*b*). Therefore, we applied single UV-light flashes to cells filled with caged cAMP (100 μM; see Methods) (Fig. 2*D* and *E*). Photolytic release of cAMP induced an increase to $122.5 \pm 2.4\%$ of control amplitude in cells from NE animals ($n = 8$, $P < 0.0001$; Fig. 2*E*), reflecting a submaximal cAMP stimulation of the channel (Lüthi & McCormick, 1999*b*). In contrast, current amplitudes in GAERS increased to only $113.8 \pm 1.3\%$ ($n = 6$, $P < 0.025$ compared to NE; Fig. 2*E*) after photolysis of caged cAMP. These values are ~40% smaller compared to NE.

To assess whether or not this difference reflected acquired alterations in channel function due to chronic epilepsy, we repeated the flash photolysis experiment in young animals (P19–24) which have not yet developed SWDs. Photolytic release of cAMP induced an increase to $118.5 \pm 2.9\%$ of control current in cells from the NE strain ($n = 12$, $P < 0.0001$), whereas the increase was only $110.8 \pm 1.4\%$ in cells from GAERS ($n = 12$, $P < 0.05$ compared to NE; Fig. 2*D* and *E*). Moreover, cells from young animals (both the GAERS and the NE strain) showed similar maximal shifts in current–voltage dependence when 1 mM 8Br-cAMP was bath-applied (data not shown).

Flash photolysis of caged cAMP and bath application of 8Br-cAMP does not allow determination of the free cAMP concentrations reached intracellularly. Therefore, we next assessed cAMP regulation of I_h by constructing a concentration–response curve between 8Br-cAMP, included at defined concentrations in the patch pipette, and $V_{1/2}$ values in TC cells of mature animals (see Methods). Notably, in TC cells from GAERS, the shifts induced in the concentration range between ~0.1 and 1 μM were significantly smaller than those in cells from NE animals (Fig. 2*F* and *G*). For example, including 0.1 μM 8Br-cAMP yielded values of $V_{1/2} = -84.1 \pm 1.0$ mV in NE TC cells ($n = 9$), while GAERS TC cells had a $V_{1/2} = -89.9 \pm 1.4$ mV ($n = 10$, $P < 0.01$), indicating that the voltage dependence of I_h was not appreciably affected in GAERS. Furthermore, whereas 1 μM 8Br-cAMP produced a near-maximal shift of $V_{1/2}$ in NE TC cells (-76.1 ± 1.8 mV, $n = 5$), the voltage dependence of GAERS TC cells was only partially shifted ($V_{1/2} = -80.7 \pm 0.5$ mV, $n = 7$, $P < 0.05$). Fitting a Hill equation to the concentration–response curve yielded a half-maximal concentration of 0.16 ± 0.07 μM 8Br-cAMP for NE cells, whereas a similar shift in GAERS required 0.81 ± 0.38 μM. These experiments reveal that I_h in TC cells from GAERS shows a distinctly reduced sensitivity to submaximal concentrations of cAMP, consistent with the results obtained via flash photolysis and with a recent report on pre-epileptic TC cells in the dorsal lateral geniculate nucleus of the WAG/Rij strain (Budde *et al.* 2005). Moreover, this reduced I_h sensitivity to non-saturating cAMP concentrations precedes the onset of the seizures. This supports a causal role of this defect in SWD generation, and excludes the possibility that these changes are compensatory or secondary to the seizures.

Altered expression of HCN channel subunit mRNA in thalamocortical neurones of GAERS

The decreased sensitivity of I_h to cAMP in GAERS raised the possibility that the subunit composition of the channel was altered, such that weakly cAMP-sensitive isoforms were expressed at relatively higher levels. To test this hypothesis, we examined the expression of the three HCN channel isoforms present in thalamus. Messenger RNA levels of the cAMP-sensitive HCN channel subunit most abundant in thalamus, HCN2, did not differ between mature GAERS and NE animals in either the Vpm or the reticular nucleus (Rtn) (Fig. 3*A–C*). For example, in Vpm, mRNA levels were 71 ± 0.4 and 70 ± 0.4 nCi g^{-1} in NE rats and GAERS, respectively. Similarly, no difference was found in the expression of the other abundant, cAMP-sensitive HCN channel isoform, HCN4 (Fig. 3*D–F*). However, a significant, ~59% increase in the expression levels of the relatively cAMP-insensitive HCN1 channel isoform was found in the GAERS Vpm (34.1 ± 3.3 nCi g^{-1}) compared with mature NE rats (21.5 ± 0.79 nCi g^{-1}, $P < 0.025$, *t* test with Welch's correction) (Fig. 4). Similar changes were found also in the Rtn (31.17 ± 1.3 *versus* 24.33 ± 1.47 nCi g^{-1}, $P < 0.01$). Note that the increased expression of HCN1 channels

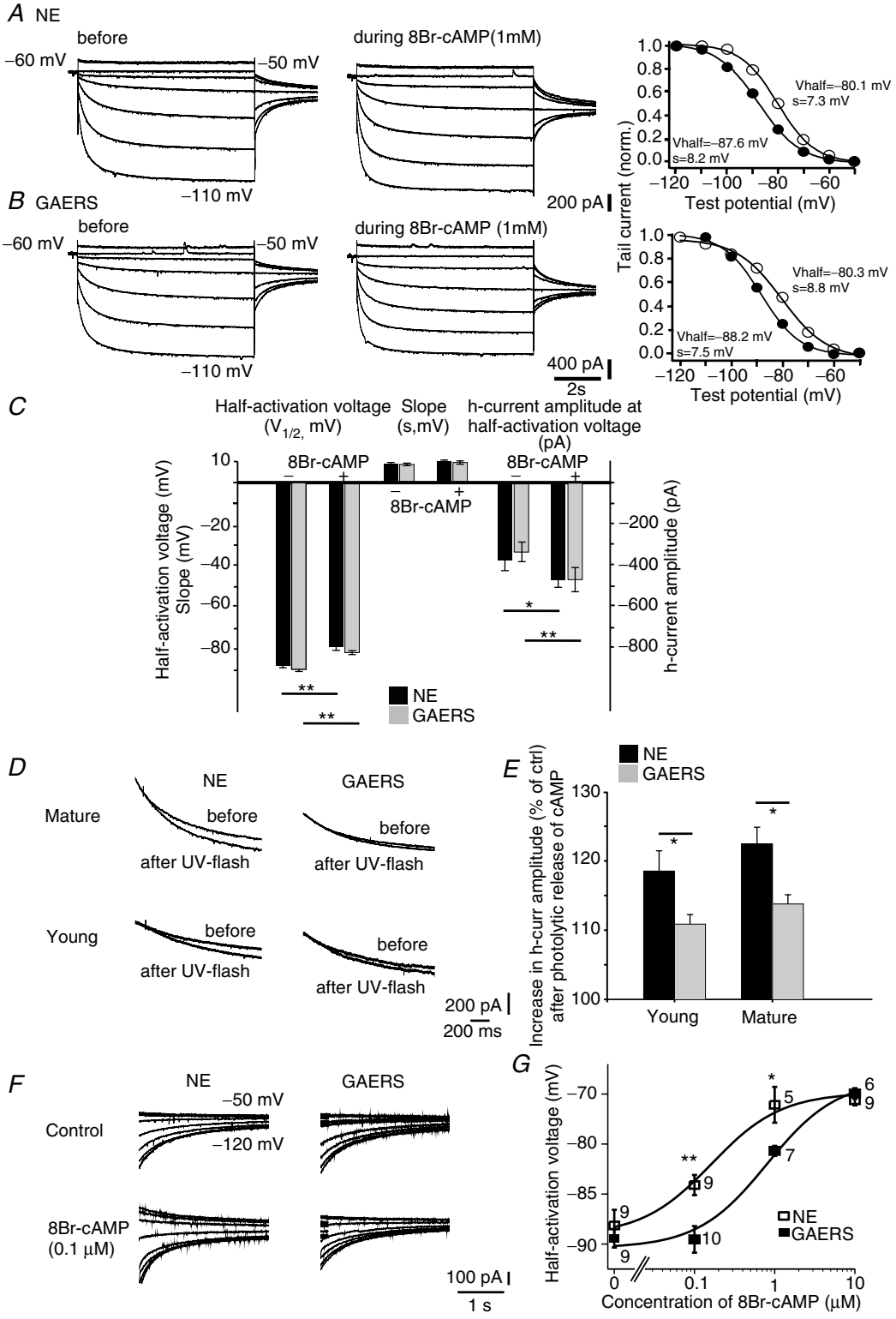

Figure 2. The I_h of GAERS TC cells shows a diminished sensitivity to submaximal, near-physiological cAMP pulses, but not to saturating cAMP concentrations

A and *B*, current responses of mature TC cells from a NE rat (*A*) and a GAERS (*B*) to increasing negative test voltages (test voltages −50 mV and −110 mV are indicated next to the traces) before, and in the continuous presence of, 8Br-cAMP at a concentration of 1 mM. Corresponding activation curves, constructed from tail currents evoked at −80 mV (see Methods), are shown to the right. Thick lines represent the optimal fit of a Boltzmann curve, with the resulting values for the half-activation voltage (V_{half}) and the slope (*s*) indicated next to them. Filled and

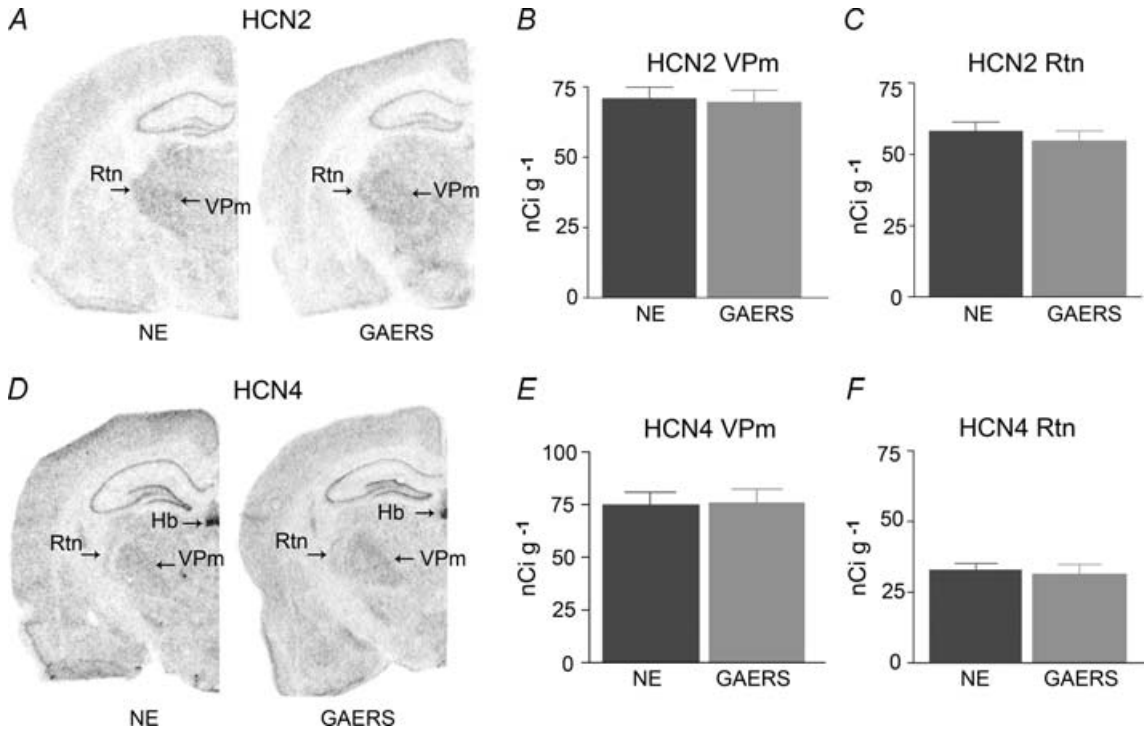

Figure 3. Expression of HCN2 (top row) and HCN4 (bottom row) mRNA in selected thalamic nuclei does not differ in GAERS and NE controls

A, representative coronal brain sections at the level of the thalamus that have been subjected to quantitative *in situ* hybridization for the HCN2 channel isoform. The preferential expression of this isoform in thalamus is apparent. *B* and *C,* quantitative analysis of mRNA expression levels of HCN2 channels comparing GAERS to NE rats. The strains are not distinguishable in the expression of this isoform. *D,* representative sections of GAERS and NE rat brain for HCN4 mRNA expression. Note the relatively lower expression of this isoform in the Rtn, and the typical signal of HCN4 in the habenula, supporting the specificity of the probes. *E* and *F*, quantitative analyses of HCN4 mRNA expression indicate the absence of significant differences in GAERS *versus* NE. Hb = habenula.

was specific to thalamic nuclei: mRNA expression levels of this isoform were similar in somatosensory cortical layer V of GAERS and NE control rats (61.8 ± 5.2 and 64.2 ± 5.0 nCi g^{-1} in controls and GAERS, respectively, NS). The increased HCN1 isoform expression in select thalamic nuclei, with maintained levels of HCN2, is consistent with the overall reduced sensitivity of the resulting complement of cellular HCN channels to cAMP.

The Western blot analyses, carried out on whole thalamus samples, confirmed that levels of HCN2 channel expression in this region are much higher than those of HCN1. In addition, HCN2 protein levels were similar in

open circles represent values before and during 8Br-cAMP application, respectively. *C*, bar graph showing the pooled data for $V_{1/2}$, for *s*, and for the current amplitude at −90 mV before, and in the continuous presence of 8Br-cAMP (1 mM). Except for *s*, 8Br-cAMP significantly altered all control values. The changes in all three parameters were indistinguishable between mature NE ($n = 8$) and GAERS ($n = 7$) TC cells. *D*, responses of I_h to photolytic release of caged cAMP in mature (top row) and young (bottom row) NE animals and GAERS. Overlay of current responses to 30 mV hyperpolarizing voltage steps before and after application of a UV flash in cells perfused with caged cAMP (see Methods). Holding potential was −60 mV. For clarity, only current relaxations during the hyperpolarizing voltage step are shown; passive responses to the step voltage were blanked. *E*, bar graph showing the percentage increase in current response in young and mature NE animals (young: $n = 12$; mature: $n = 8$) and GAERS (young: $n = 12$; mature: $n = 12$). *F*, representative tail currents obtained from TC cells in the absence of (control) or during perfusion of the cellular interior with 0.1 μM 8Br-cAMP. The same voltage protocol as in *A* was used, voltage steps applied prior to evoking tail currents are indicated next to the traces, and tails were evoked at −75 mV. *G*, concentration–response curve for the effect of 8Br-cAMP on the half-activation voltage. The number of recorded cells is indicated next to the symbols. Fitting of the Hill equation was achieved by fixing the Hill coefficient to 1 (see Methods), yielding a ∼5-fold increase of half maximal concentration of 8Br-cAMP in GAERS. $^*P < 0.05$, $^{**}P < 0.01$.

Table 1. Values of membrane properties of sag and nonsag TC neurones recorded *in vivo* in GAERS and NE rats

	Resting MP (mV)	peak IR (MΩ)
Sag cells		
GAERS ($n = 42$)	-59.5 ± 0.6	25.1 ± 1.1
	GAERS/NE, NS	GAERS/NE, NS
	sag/non-sag, $P < 0.01$	sag/non-sag, $P < 0.01$
NE ($n = 28$)	-58.5 ± 0.6	23.5 ± 1.3
	sag/non-sag, $P < 0.05$	sag/non-sag, $P < 0.01$
Non-sag cells		
GAERS ($n = 13$)	-65.2 ± 1.7	18.2 ± 1.8
	GAERS/NE, NS	GAERS/NE, NS
NE (n = 17)	-63.7 ± 1.8	18.2 ± 1.3

IR = input resistance; MP = membrane potential.

NE and GAERS rats, being 148.7 ± 8.9 and 156.9 ± 9.2 HCN/actin OD units in GAERS and NE rats, respectively. HCN1 isoform protein levels were 56.4 ± 8.0 HCN/actin OD units in GAERS, and 54.6 ± 6.1 HCN/actin OD units in the NE rats. The apparent lack of up-regulation of HCN1 channel protein in the GAERS rats is probably a result of the fact that the whole thalamus was sampled in the Western blot procedure. The dilution of channel protein in the total thalamic sample may mask potential differences that are exclusive to thalamic subregions strongly involved in SWDs.

Maintained I_h-mediated afterdepolarizations in fully epileptic mature GAERS

We next queried whether the decreased cAMP sensitivity of I_h in TC cells from GAERS translates into an altered physiological regulation of I_h. We focused here on a slow, activity-dependent up-regulation of I_h that induces the cessation of synchronized oscillations via a persistent ADP (Bal & McCormick, 1996). This ADP reflects the combined influence of Ca^{2+} entry through voltage-gated Ca^{2+} channels, Ca^{2+}-dependent cAMP synthesis, HCN channel voltage gating and binding to cAMP, and the

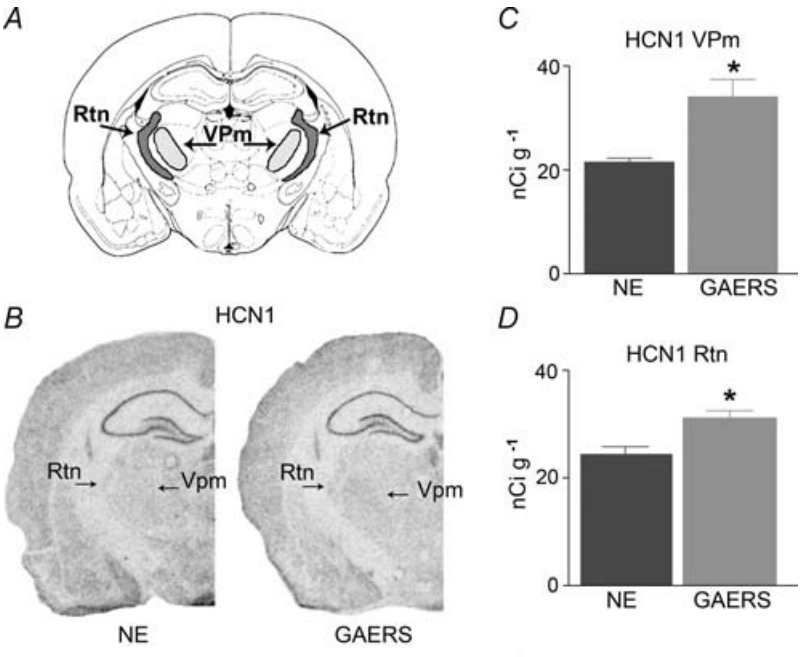

Figure 4. Quantitative analysis of the expression of the HCN1 channel mRNA in thalamic neurones of GAERS and NE rats
A, a schematic diagram showing the level where coronal sections from brains of GAERS and NE control rats were obtained for *in situ* hybridization. *B*, representative sections from GAERS and NE rats. Although HCN1 channel expression in the thalamus is significantly lower than that of the HCN2 isoform, the darker *in situ* hybridization signal over the Vpm and Rtn is apparent in the GAERS brain. Note the robust expression of HCN1 in the principal cell layers of the hippocampus of both strains. *C*, quantitative analysis reveals a 59% increase in HCN1 mRNA levels in GAERS Vpm. *D*, quantitative analysis shows a more modest increase of HCN1 mRNA in the Rtn ($n = 5$ per group). $^*P < 0.05$ (see Methods).

degradation of cAMP by phosphodiesterases (Lüthi & McCormick, 1999*b*; Wang *et al.* 2002). The reduced sensitivity of I_h to cAMP in GAERS predicted smaller ADPs following repetitive rebound Ca^{2+} spike generation.

Cells were held between −58 and −64 mV, close to their resting membrane potentials (−65.7 ± 0.7 mV for NE, $n = 25$; −63.5 ± 1.2 mV for GAERS, $n = 24$; NS), and 16 negative current pulses (−0.3 to −0.9 nA), each lasting 120 ms, were injected at 4 Hz (Fig. 5*A* and *D*, bottom), a protocol producing maximal ADPs (Lüthi & McCormick, 1999*a*). The resulting ADP amplitude was measured relative to baseline 2 s after termination of these current injections to minimize the contribution of a rapidly decaying depolarization immediately after the end of the pulses (Fig. 5*A*). These ADPs, albeit small, efficiently attenuated spontaneous δ-oscillations that were observed in some recordings ($n = 2$; Fig. 5*B*), documenting the efficacy of small membrane depolarizations in preventing or terminating burst discharges in TC cells. In mature NE animals, ADP amplitudes were 2.3 ± 0.2 mV ($n = 24$; Fig. 5*A* and *F*) and these were reduced > 80% by extracellular application of the I_h blocker Cs^+ (3 mM, $n = 4$, $P < 0.05$; Fig. 5*C*). Interestingly, amplitudes of ADPs in mature GAERS did not differ from those in age-matched controls (2.8 ± 0.2 mV, $n = 24$; Fig. 5*D* and *F*); and ADPs sufficed to dampen intrinsic rhythmic activity ($n = 4$; Fig. 5*E*) and they were largely blocked by extracellular Cs^+ ($n = 3$, $P < 0.05$, data not shown).

In contrast to cells from mature animals, ADPs elicited in cells from pre-epileptic GAERS and young NE animals were too small for further analysis (1.7 ± 0.2 mV, $n = 8$; for both NE and GAERS, $P < 0.001$ compared to adults), indicating insufficient maturation of the functional interaction between Ca^{2+} spikes and I_h before the onset of SWDs. These data suggest that both NE animals and GAERS go through a developmental enhancement of Ca^{2+}-induced persistent I_h up-regulation, and that, in GAERS, this occurs in the face of enduring reduction of cAMP regulation of I_h.

Unaltered cAMP turnover in TC neurones of mature GAERS

Which mechanisms in the mature GAERS could overcome the functional deficits of HCN channels and facilitate the generation of ADPs? Higher cAMP levels in the vicinity of the HCN channels in GAERS could result from a reduced degradation of cAMP.

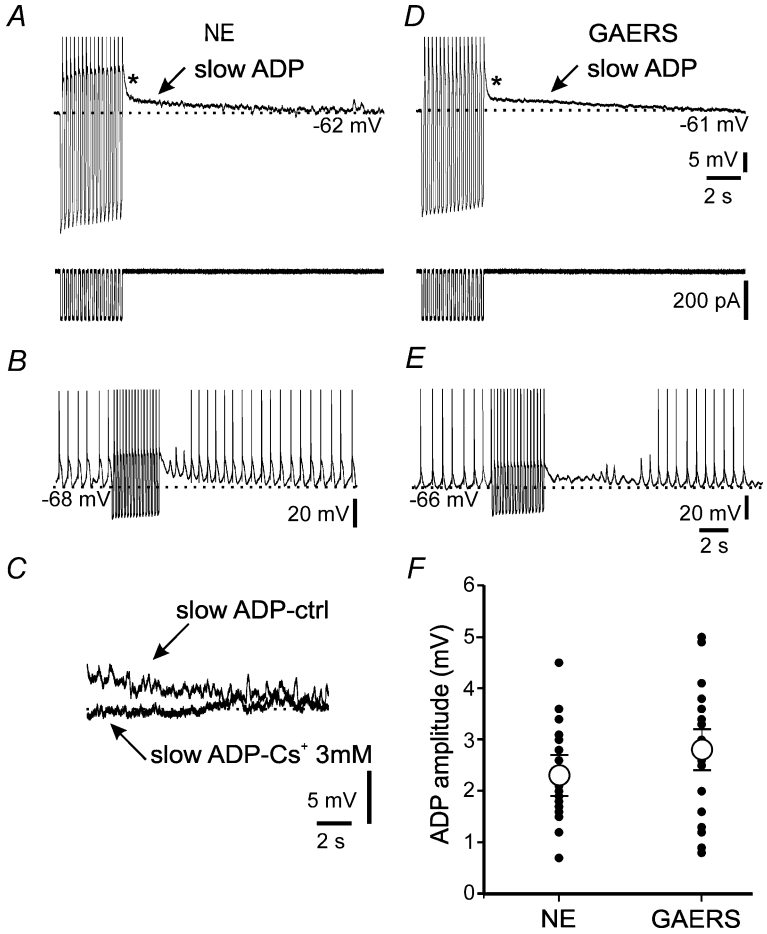

Figure 5. Mature GAERS TC cells generate unaltered afterdepolarizations (ADPs)
A and *D*, representative ADPs (arrow) found in TC cells from mature NE rats (*A*) and GAERS (*D*). The asterisk (*) denotes a fast ADP that is not mediated by I_h. The current injection protocols used to elicit the ADPs in *A* and *D* are shown below the traces. *B* and *E,* cells showing spontaneous clock-like δ-oscillations in a TC cell of a NE animal (*B*) and a GAERS (*E*). Note the attenuation of these oscillations during the ADP and their gradual reappearance. *C,* the slow ADP, shown here for a NE control (slow ADP-ctrl), is blocked in the presence of 3 mM Cs^+ in the superfusing solution (slow ADP – Cs^+ 3 mM). *F,* pooled values of ADP amplitudes for all experiments ($n = 24$ for both strains). Filled circles denote results of individual experiments, and are sometimes superimposed on each other. Average values (open circles) were not significantly different (NS).

To obtain a measure of cAMP degradation, we examined the time course of the photolytic responses in mature GAERS and NE controls. In both cases, responses to the UV-light flash peaked within the first voltage step after flashing (see Methods) and then gradually decayed back to baseline levels. In both NE and GAERS TC neurones, recovery was complete within six current responses obtained at 4 s intervals after flash application, characterized by a time constant of 11.2 ± 1.2 s for NE and 7.9 ± 1.3 s for GAERS ($n = 7$ for NE, $n = 6$ for GAERS, NS; Fig. 6), similar to previous observations (Lüthi & McCormick, 1999*b*). These data indicate that unbinding and/or diffusion/degradation of cAMP are not altered in mature GAERS neurones, and therefore cannot account for the preserved ADP amplitudes.

Enhanced intracellular Ca^{2+} accumulation in GAERS neurones during repetitive low-threshold Ca^{2+} spikes

Molecular analyses have shown that expression of Ca^{2+} channel subunits in rat decreases by ~25% between 2 weeks and 2–3 months of age, but this reduction is less pronounced in GAERS (Guyon *et al.* 1993; Talley *et al.* 2000). In addition, increased amplitudes of LT Ca^{2+} currents in TC neurones were reported in several mouse models of SWDs (Zhang *et al.* 2002; Song *et al.* 2004). Therefore, Ca^{2+} entry via these channels might be altered in GAERS, and contribute to the normalization of the ADPs. To test this possibility, we performed simultaneous electrophysiological and Ca^{2+} imaging in cells filled with the Ca^{2+} indicator dye Oregon Green Bapta-2 (75 μM, see Methods). Changes in fluorescence were monitored following rebound Ca^{2+} spikes evoked by repetitive hyperpolarizing pulses. These Ca^{2+} spikes induced a progressive increase in the fluorescence signal that summated to reach a maximal average value of $115 \pm 3\%$ of baseline after 8–16 rebound bursts ($n = 8$; Fig. 7*A*, *B* and *D*). At the end of the stimulation protocol, the fluorescence signal returned to baseline within seconds (monoexponental decay: $\tau = 2.6 \pm 0.5$ s, $n = 8$). These results are in agreement with observations from Budde *et al.* (2000). To confirm that our stimulation protocol did not saturate the Ca^{2+} indicator and permitted recording larger fluorescence changes, positive current injections (+0.5 nA) were used to depolarize cells to suprathreshold voltages. Under these conditions, the increases in fluorescence recorded were about 2-fold larger ($\Delta F/F = 132 \pm 2\%$, $P < 0.005$; Fig. 7*C* and *D*), but decayed on a similar time scale ($\tau = 1.8 \pm 0.2$ s, $n = 5$, NS).

We obtained fluorescence data from both somatic and proximal dendritic compartments, where T-type Ca^{2+} channels are expressed and colocalized with HCN channels (Stuart & Williams, 2000). Signals evoked by hyperpolarizing pulses were comparable in amplitude at the end of the train in both regions ($\Delta F/F = 115 \pm 3\%$ in the soma, $n = 8$, $\Delta F/F = 119 \pm 3\%$ in dendrites, $n = 6$,

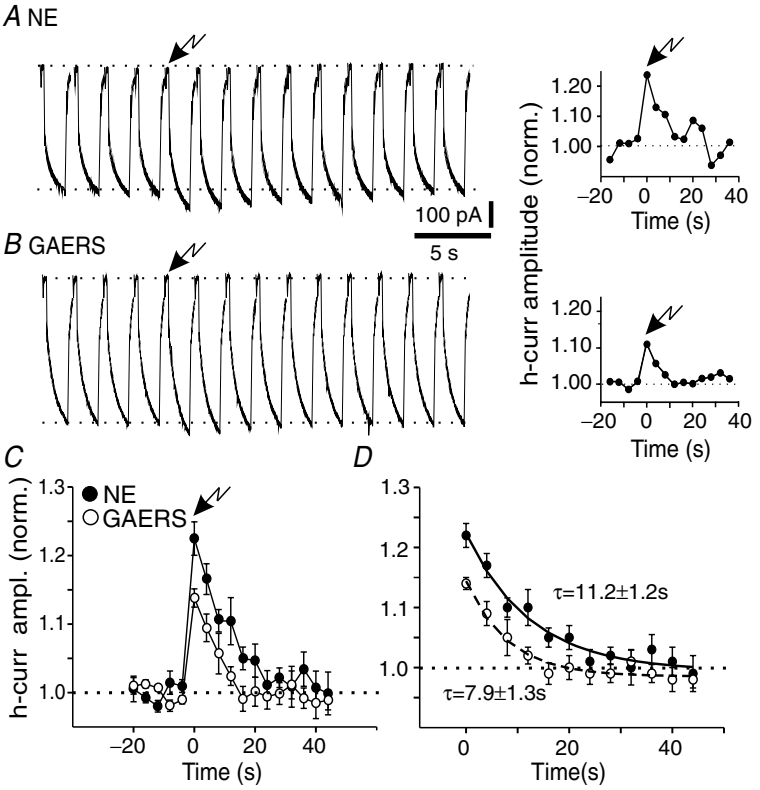

Figure 6. Unaltered decay time course of current enhancement following photolytic release of caged cAMP
A and *B*, representative responses in cells derived from mature NE animals and GAERS on the left, with normalized plot of current amplitude presented to the right. Voltage protocol involved a −30 mV hyperpolarizing step from −60 mV, flash application occurred after 4 control responses (arrow, time 0 in the graphs). *C*, normalized, averaged responses in NE (filled circles, $n = 7$) and GAERS (open circles, $n = 6$) to repetitive 30 mV hyperpolarizing steps, UV-flash application occurred at time 0 (arrow). Note decreased response in cells from GAERS ($P < 0.02$ at the peak of the cAMP-induced effect). *D*, monoexponential fitting of the decay time course of the current responses after photolysis of caged cAMP. The time constant values indicated next to the traces are the mean ± S.E.M. values obtained by exponential fitting of the traces from individual cells (see Methods), and these values were not significantly different (NS).

NS; Fig. 7*B* and *D*), but dendritic signals decayed more rapidly ($\tau = 1.2 \pm 0.04$ s, $n = 6$, $P < 0.05$). Depolarizing pulses evoked comparable fluorescent signals in the two compartments (Fig. 7*C* and *D*), with dendritic signals again decaying slightly faster ($\tau = 1.2 \pm 0.1$ s, $n = 4$, $P < 0.05$).

Ca^{2+} levels were markedly elevated in somata and dendrites of GAERS compared with NE cells when eight or more hyperpolarizing pulses were injected ($\Delta F/F = 123$–125%, $n = 8$, $\Delta F/F = 134$–138%, $n = 5$, in somata and dendrites, respectively, $P < 0.05$ compared to NE; Fig. 7*B* and *D*), while time constants of decay obtained by monoexponential ($\tau = 1.7 \pm 0.1$ s and 1.4 ± 0.1 s in somata and dendrites, respectively, NS) or biexponential fitting (data not shown, NS) were unaltered. GAERS and NE cells did not differ in intracellular Ca^{2+} concentrations after depolarizing pulses ($n = 6$ for somatic, $n = 4$ for dendritic recordings, NS; Fig. 7*C* and *D*). These data indicate that the summation of Ca^{2+} transients induced by repetitive LT Ca^{2+} spikes in GAERS cells is selectively augmented, and can potentiate Ca^{2+}-dependent I_h up-regulation, thus contributing to ADP normalization.

Discussion

In this study, we addressed the role of I_h during both epileptogenesis and the chronically epileptic state of the GAERS. Importantly, we focused on I_h in the somatosensory thalamus that constitutes the primary thalamic area generating SWDs in rat models of absence epilepsy (Vergnes *et al.* 1990; Seidenbecher *et al.* 1998;

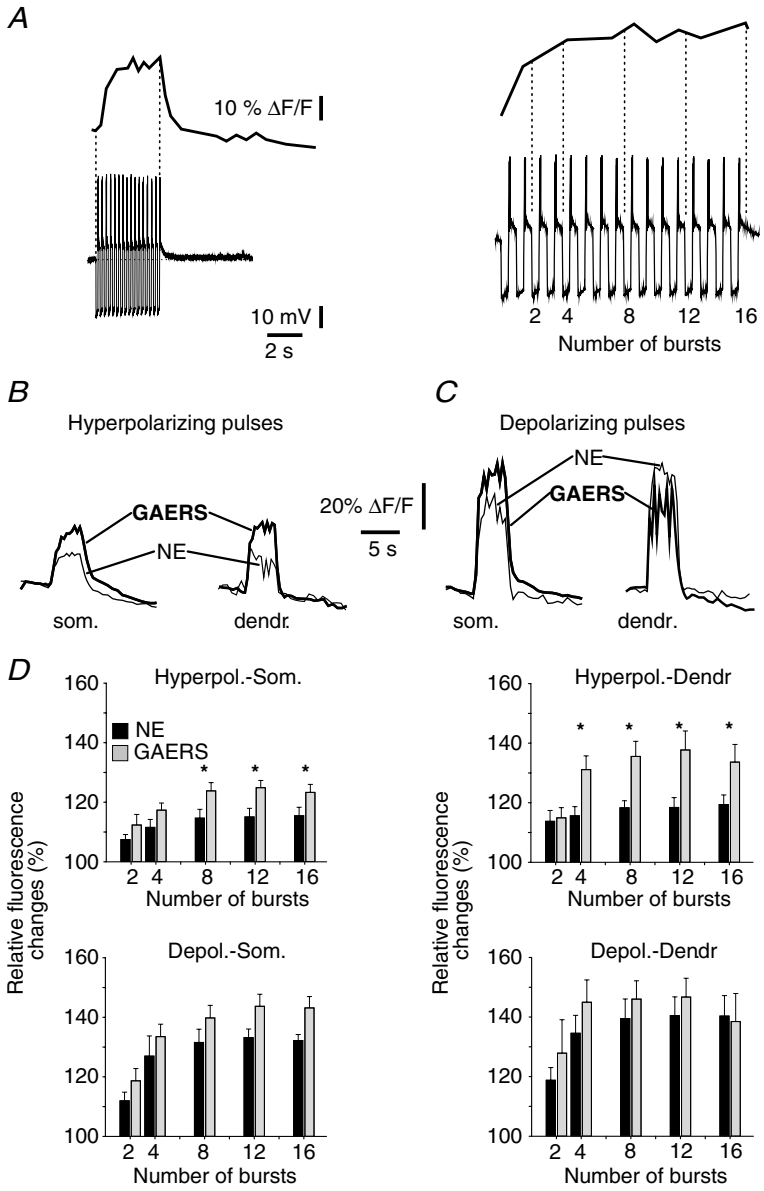

Figure 7. Repetitive hyperpolarizing current pulses evoke greater intracellular Ca^{2+} increases in GAERS neurones
A, left, representative sweeps showing the relative fluorescence changes evoked after repetitive rebound Ca^{2+} bursting in a cell from a NE rat. Right, expanded portion of the trace illustrating the time sections (vertical dotted lines) within which Ca^{2+} signals were averaged and compared. *B*, Ca^{2+} transients recorded in somatic (som.) and dendritic (dendr.) regions after somatic injection of hyperpolarizing currents to induce rebound bursting. Transients are averages of 5 successive sweeps for cells from a NE animal (thin line) and a GAERS (thick line). *C*, as in *B*, but depolarizing current pulses were injected. *D*, top, pooled data showing the relative changes in fluorescence evoked after repetitive hyperpolarizing pulses and recorded from somatic (Hyperpol.-Som., $n = 8$ for both NE and GAERS) or dendritic (Hyperpol.-Dendr., $n = 6$ for NE, $n = 5$ for GAERS) regions. Bottom, as top but for depolarizing somatic pulses recorded in soma (Depol.-Som., $n = 5$ for NE, $n = 6$ for GAERS) or in dendrites (Depol.-Dendr., $n = 4$ for both NE and GAERS). $^*P < 0.05$.

Renier & Coenen, 2000; Manning *et al.* 2004; Nersesyan *et al.* 2004; Budde *et al.* 2005). This approach allowed us to evaluate the contribution of inherited (or developmentally determined) and acquired changes in current properties to the pathogenesis of generalized epilepsy.

The principal findings presented here are: (1) basal electrophysiological characteristics, including resting membrane potential and voltage gating of I_h, were unaltered in TC cells of adult GAERS, both *in vivo* and *in vitro*; (2) during both pre-epileptic and chronic epileptic stages, I_h was less sensitive to cAMP when the nucleotide was delivered at non-saturating doses; (3) a marked increase in mRNA levels of the relatively cAMP-insensitive HCN1 isoform occurred in the GAERS thalamus, without significant changes in cAMP-sensitive HCN2 and HCN4; (4) ADP amplitudes were normal in mature GAERS, despite the enduring, reduced cAMP sensitivity of I_h and the up-regulation of HCN1 subunit expression; (5) compensatory mechanisms, likely restoring ADP amplitude, involved enhanced Ca^{2+} accumulation in mature GAERS TC cells resulting from LT Ca^{2+} spikes. In summary, I_h may play a dual role in the GAERS epilepsy. Abnormal regulation of this current accompanies the pathogenesis of this absence epilepsy, and appears to trigger adaptive responses to restore I_h functions that are important for the termination of synchronous network activity.

Our work further highlights that neuronal networks are exquisitely sensitive to imbalances in I_h regulation (Santoro & Baram, 2003; Frère *et al.* 2004). Indeed, prior studies have identified comparatively small changes in current amplitude around resting membrane potentials (Di Pasquale *et al.* 1997) or in current–voltage dependence (Chen *et al.* 2001*a*; Budde *et al.* 2005) in rodent models of epilepsy that were accompanied by major increases in the propensity of neuronal networks to generate seizures.

Role of altered I_h function in the development of absence epilepsy

We identified a lowered sensitivity of I_h to near-physiological, phasic cAMP pulses in pre-epileptic TC cells of GAERS, similar to a previous report in pre-epileptic WAG/Rij rats (Budde *et al.* 2005). Therefore, although we did not quantify HCN mRNA levels in the pre-epileptic state, our findings support the idea that abnormal cAMP sensitivity of HCN channels in thalamus may be a common denominator of rodent absence epilepsy during pre-epileptic stages. In pre-epileptic GAERS, the gating of I_h by cAMP will attenuate a depolarizing contribution to the resting membrane potential. To what extent this attenuation shifts the percentage of TC cells towards a more hyperpolarized stage *in vivo*, eventually leading to SWDs (Pinault *et al.* 1998; Seidenbecher *et al.* 1998; Pinault, 2003) remains to be determined. One important contribution is that weakened cAMP actions contribute to the facilitation of burst discharge in pre-epileptic TC cells (Budde *et al.* 2005), thereby furthering the spontaneous synchronization of TC and Rtn neurones. The decreased efficacy of cAMP could result from a genetically determined predisposition of the GAERS strain (Rudolf *et al.* 2004), but might also be a consequence of an abnormal development of the TC network. For example, levels of neuronal and glial enzymes involved in the turnover of glutamate are reduced in TC networks during pre-epileptic stages (Dutuit *et al.* 2000, 2002), promoting elevated concentrations of ambient glutamate and therefore altered regulation of I_h (van Welie *et al.* 2004).

Of note, changes in functional and molecular properties of cortical I_h, particularly a decreased HCN1 expression, have been identified in animal models of SWDs (Di Pasquale *et al.* 1997; Strauss *et al.* 2004). Here, HCN1 or HCN2 channel expression in somatosensory cortex remained unchanged, rendering unlikely a major contribution of abnormal cortical I_h in the pathological condition of GAERS. Although potential functional changes in selected cortical neurons cannot be excluded, the observation that mice deficient in the major thalamic (Ludwig *et al.* 2003), but not in the most abundant cortical, isoform (Nolan *et al.* 2004) have spontaneous SWDs points to a major role of thalamic I_h in the susceptibility to SWDs.

Molecular composition of thalamic HCN channels in GAERS

The mRNA expression of HCN1, the subunit with the weakest sensitivity to cAMP, was augmented in adult GAERS, raising the question of how increased HCN1 protein modifies cAMP sensitivity of native HCN channels, without altering resting membrane potential and basal current amplitudes. Assuming that protein expression of HCN1 correlates quantitatively with the mRNA levels (Brewster *et al.* 2005, 2006) in single thalamic nuclei, the contribution of HCN1 to the total complement of HCN channels in Vpm is 12.5% in controls and ∼20% in GAERS. In addition, voltage gating of I_h around resting potentials is small (∼10%, see Fig. 2*A*), suggesting that increased HCN1 has minimal effects on the resting state. However, a selective reduction of cAMP sensitivity in GAERS HCN channels may derive from enhanced heteromerization, driven by increased relative HCN1 subunit abundance (Brewster *et al.* 2005). HCN1/HCN2 heteromers and HCN2 homomers have a cAMP concentration–response curve with a similar maximum, yet heteromers show a weaker shift at

subsaturing concentrations (Chen *et al.* 2001*b*), thereby producing channels with properties approximating those found in GAERS. The findings fit less well with HCN1/HCN4 heteromerization, because the maximal shift of HCN1/HCN4 heteromers is markedly smaller than that of HCN4 homomers (Altomare *et al.* 2003), and HCN4 contributes to thalamic I_h (Seifert *et al.* 1999). Thus, the impact of HCN1-containing heteromers on cAMP sensitivity of whole-cell currents may depend on the type and amount of heteromers generated, as well as be influenced by a number of proteins interacting with HCN channels (Yu *et al.* 2001; Decher *et al.* 2003; Gravante *et al.* 2004; Santoro *et al.* 2004; Vasilyev & Barish, 2004). Altered expression or function of these (or other) proteins might influence, and perhaps disproportionately strengthen, the function and localization of HCN1-containing channels in GAERS TC cells.

Role of altered I_h function in chronic epilepsy

Chronic epilepsy in mature animals did not modify the relative proportions of TC cell subtypes described *in vivo* (Pinault, 2003). However, the reduced cAMP sensitivity of I_h, accompanied by an elevated HCN1 mRNA expression, persisted in the chronic state of epilepsy. Thus, the changes in thalamic I_h function, already present during pre-epileptic stages, appear to be unaltered by the onset of epileptic activity. This is in contrast to other experimental models, in which a single seizure episode markedly and persistently affects current properties and subunit expression (Chen *et al.* 2001*a*; Brewster *et al.* 2002; Shah *et al.* 2004). Moreover, chronic epilepsy in this study was accompanied by compensatory adjustments of a regulatory mode of I_h that specifically helps to organize the hyperpolarization of TC cells typical for SWDs. An attractive putative mechanism for such a compensatory effect involves augmented Ca^{2+} currents. In addition to enhanced LT current expression in animal models of SWDs (Guyon *et al.* 1993; Talley *et al.* 2000; Zhang *et al.* 2002), T-type channel expression is persistently enhanced by pathological hyperactivity, either due to experimental seizures (Beck *et al.* 1998; Su *et al.* 2002), or to genetic interference with Ca^{2+} channel activity or neurotransmitter release (Song *et al.* 2004; Zhang *et al.* 2004). Here, we found a greater temporal summation of Ca^{2+} signals evoked by repetitive opening of the T-type Ca^{2+} channels in GAERS at frequencies approximating those in SWDs. However, no overt changes occurred after single or few spikes. This suggests that, rather than the expression of T-channels, the intracellular clearance of Ca^{2+} ions entering through these channels might be diminished in GAERS, for example through reduced expression of Ca^{2+}-binding proteins (Montpied *et al.* 1995) known to be expressed in TC cells (Meuth *et al.* 2005). Although our analysis did not reveal differences in the decay kinetics of the Ca^{2+} transients, an indicator for changes in endogenous Ca^{2+} buffering or extrusion mechanisms, further analysis of the expression patterns and functional roles of endogenous Ca^{2+}-binding proteins is required to elucidate the mechanisms underlying enhanced Ca^{2+} accumulation in GAERS TC cells.

Enhanced Ca^{2+} influx through T-channels has been implicated in augmented transcription factor activity in mouse models of SWDs (Ishige *et al.* 2001), suggesting an involvement of T-current-mediated Ca^{2+} signalling in the molecular mechanisms underlying SWDs. In GAERS, we propose that elevated levels of free Ca^{2+} in the vicinity of T-type Ca^{2+} channels should facilitate the stimulation of Ca^{2+}-sensitive adenylyl cyclases (Cooper, 2003), thereby promoting I_h up-regulation (Lüthi & McCormick, 1999*b*). Application of currently emerging cAMP imaging techniques to GAERS TC cells would represent a most direct way to test this possibility (Vincent & Brusciano, 2001). We excluded decreased cAMP degradation as a mechanism stabilizing ADPs, although the possibility remains that adenylyl cyclases activated by Ca^{2+} are increasingly expressed or more active in GAERS.

The present results further substantiate the critical role of thalamic HCN channels in the involvement of thalamic networks in SWDs (Pinault *et al.* 1998, 2003; Seidenbecher *et al.* 1998; Meeren *et al.* 2005). We demonstrate that activity-dependent alterations in HCN channel function accompany epileptogenesis, while basal current properties are minimally affected. In addition, we show that imbalances in HCN channel transcription are found in chronic epilepsy, rendering HCN channels candidates for the growing family of ion channels underlying transcriptional channelopathies (Waxman, 2001). A reduced HCN1 protein was previously found in cortical neurones in the WAG/Rij absence model (Strauss *et al.* 2004). Thus, the construction of functional HCN channels may be affected at multiple levels and in a cell-type specific manner in TC networks generating SWDs. Moreover, while thalamic neurones use homeostatic mechanisms to compensate for deficits at the channel level, cortical abnormalities persist through adulthood (Strauss *et al.* 2004). This differential adaptation may explain the persistence of SWDs in adult rodent models, where cortical hyperactivity and exacerbated burst discharges of Rtn cells initiate SWDs (Slaght *et al.* 2002; Manning *et al.* 2004; Meeren *et al.* 2005).

References

Altomare C, Terragni B, Brioschi C, Milanesi R, Pagliuca C, Viscomi C, Moroni A, Baruscotti M & DiFrancesco D (2003). Heteromeric HCN1–HCN4 channels: a comparison with native pacemaker channels from the rabbit sinoatrial node. *J Physiol* **549**, 347–359.

Bal T & McCormick DA (1996). What stops synchronized thalamocortical oscillations? *Neuron* **17**, 297–308.

Beck H, Steffens R, Elger CE & Heinemann U (1998). Voltage-dependent Ca^{2+} currents in epilepsy. *Epilepsy Res* **32**, 321–332.

Bender RA, Dubé C & Baram TZ (2004). Febrile seizures and mechanisms of epileptogenesis: insights from an animal model. *Adv Exp Med Biol* **548**, 213–225.

Bender RA, Soleymani SV, Brewster AL, Nguyen ST, Beck H, Mathern GW & Baram TZ (2003). Enhanced expression of a specific hyperpolarization-activated cyclic nucleotide-gated cation channel (HCN) in surviving dentate gyrus granule cells of human and experimental epileptic hippocampus. *J Neurosci* **23**, 6826–6836.

Brewster A, Bender RA, Chen Y, Dube C, Eghbal-Ahmadi M & Baram TZ (2002). Developmental febrile seizures modulate hippocampal gene expression of hyperpolarization-activated channels in an isoform- and cell-specific manner. *J Neurosci* **22**, 4591–4599.

Brewster A, Bernard JA, Gall CM & Baram TZ (2005). Formation of heteromeric hyperpolarization-activated cyclic nucleotide-gated (HCN) channels in the hippocampus is regulated by developmental seizures. *Neurobiol Dis* **19**, 200–207.

Brewster AL, Chen Y, Bender RA, Yeh A, Shigemoto R & Baram TZ (2006). Quantitative analysis and subcellular distribution of mRNA and protein expression of the hyperpolarization-activated cyclic nucleotide-gated (HCN) channels throughout development in rat hippocampus. *Cereb Cortex* (in press).

Budde T, Caputi L, Kanyshkova T, Staak R, Abrahamczik C, Munsch T & Pape HC (2005). Impaired regulation of thalamic pacemaker channels through an imbalance of subunit expression in absence epilepsy. *J Neurosci* **25**, 9871–9882.

Budde T, Sieg F, Braunewell KH, Gundelfinger ED & Pape HC (2000). Ca^{2+}-induced Ca^{2+} release supports the relay mode of activity in thalamocortical cells. *Neuron* **26**, 483–492.

Chen K, Aradi I, Thon N, Eghbal-Ahmadi M, Baram TZ & Soltesz I (2001*a*). Persistently modified h-channels after complex febrile seizures convert the seizure-induced enhancement of inhibition to hyperexcitability. *Nat Med* **7**, 331–337.

Chen S, Wang J & Siegelbaum SA (2001*b*). Properties of hyperpolarization-activated pacemaker current defined by coassembly of HCN1 and HCN2 subunits and basal modulation by cyclic nucleotide. *J General Physiol* **117**, 491–504.

Cooper DM (2003). Molecular and cellular requirements for the regulation of adenylate cyclases by calcium. *Biochem Soc Trans* **31**, 912–915.

Decher N, Bundis F, Vajna R & Steinmeyer K (2003). KCNE2 modulates current amplitudes and activation kinetics of HCN4: influence of KCNE family members on HCN4 currents. *Pflugers Arch* **446**, 633–640.

Di Pasquale E, Keegan KD & Noebels JL (1997). Increased excitability and inward rectification in layer V cortical pyramidal neurons in the epileptic mutant mouse *Stargazer*. *J Neurophysiol* **77**, 621–631.

Dutuit M, Didier-Bazès M, Vergnes M, Mutin M, Conjard A, Akaoka H, Belin MF & Touret M (2000). Specific alteration in the expression of glial fibrillary acidic protein, glutamate dehydrogenase, and glutamine synthetase in rats with genetic absence epilepsy. *Glia* **32**, 15–24.

Dutuit M, Touret M, Szymocha R, Nehlig A, Belin MF & Didier-Bazès M (2002). Decreased expression of glutamate transporters in genetic absence epilepsy rats before seizure occurrence. *J Neurochem* **80**, 1029–1038.

Frère SGA, Kuisle M & Lüthi A (2004). Regulation of recombinant and native hyperpolarization-activated cation channels. *Mol Neurobiol* **30**, 279–306.

Gravante B, Barbuti A, Milanesi R, Zappi I, Viscomi C & DiFrancesco D (2004). Interaction of the pacemaker channel HCN1 with filamin A. *J Biol Chem* **279**, 43847–43853.

Guyon A, Vergnes M & Leresche N (1993). Thalamic low threshold calcium current in a genetic model of absence epilepsy. *Neuroreport* **4**, 1231–1234.

Holter J, Carter D, Leresche N, Crunelli V & Vincent P (2005). A TASK3 channel (KCNK9) mutation in a genetic model of absence epilepsy. *J Mol Neurosci* **25**, 37–51.

Ishige K, Endo H, Saito H & Ito Y (2001). Repeated administration of CGP 46381, a γ-aminobutyric $acid_B$ antagonist, and ethosuximide suppresses seizure-associated cyclic adenosine 3′5′ monophosphate response element- and activator protein-1 DNA-binding activities in lethargic (*lh*/*lh*) mice. *Neurosci Lett* **297**, 207–210.

Klein JP, Khera DS, Nersesyan H, Kimchi EY, Waxman SG & Blumenfeld H (2004). Dysregulation of sodium channel expression in cortical neurons in a rodent model of absence epilepsy. *Brain Res* **1000**, 102–109.

Ludwig A, Budde T, Stieber J, Moosmang S, Wahl C, Holthoff K, Langebartels A, Wotjak C, Munsch T, Zong X, Feil S, Feil R, Lancel M, Chien KR, Konnerth A, Pape HC, Biel M & Hofmann F (2003). Absence epilepsy and sinus dysrhythmia in mice lacking the pacemaker channel HCN2. *EMBO J* **22**, 216–224.

Lüthi A, Bal T & McCormick DA (1998). Periodicity of thalamic spindle waves is abolished by ZD7288, a blocker of I_h. *J Neurophysiol* **79**, 3284–3289.

Lüthi A & McCormick DA (1998*a*). H-current: properties of a neuronal and network pacemaker. *Neuron* **21**, 9–12.

Lüthi A & McCormick DA (1998*b*). Periodicity of thalamic synchronized oscillations: the role of Ca^{2+}-mediated upregulation of I_h. *Neuron* **20**, 553–563.

Lüthi A & McCormick DA (1999*a*). Ca^{2+}-mediated up-regulation of I_h in the thalamus. How cell-intrinsic ionic currents may shape network activity. *Ann N Y Acad Sci* **868**, 765–769.

Lüthi A & McCormick DA (1999*b*). Modulation of a pacemaker current through Ca^{2+}-induced stimulation of cAMP production. *Nat Neurosci* **2**, 634–641.

Manning JP, Richards DA, Leresche N, Crunelli V & Bowery NG (2004). Cortical-area specific block of genetically determined absence seizures by ethosuximide. *Neuroscience* **123**, 5–9.

Meeren H, van Luijtelaar G, Lopes da Silva F & Coenen A (2005). Evolving concepts on the pathophysiology of absence seizures: the cortical focus theory. *Arch Neurol* **62**, 371–376.

Meuth SG, Kanyshkova T, Landgraf P, Pape HC & Budde T (2005). Influence of Ca^{2+}-binding proteins and the cytoskeleton on Ca^{2+}-dependent inactivation of high-voltage activated Ca^{2+} currents in thalamocortical relay neurons. *Pflugers Arch* **450**, 111–122.

Montpied P, Winsky L, Dailey JW, Jobe PC & Jacobowitz DM (1995). Alteration in levels of expression of brain calbindin D-28k and calretinin mRNA in genetically epilepsy-prone rats. *Epilepsia* **36**, 911–921.

Neher E (1992). Correction for liquid junction potentials in patch clamp experiments. *Methods Enzymol* **207**, 123–131.

Nersesyan H, Hyder F, Rothman DL & Blumenfeld H (2004). Dynamic fMRI and EEG recordings during spike-wave seizures and generalized tonic-clonic seizures in WAG/Rij rats. *J Cereb Blood Flow Metab* **24**, 589–599.

Nolan MF, Malleret G, Dudman JT, Buhl DL, Santoro B, Gibbs E, Vronskaya S, Buzsáki G, Siegelbaum SA, Kandel ER & Morozov A (2004). A behavioral role for dendritic integration: HCN1 channels constrain spatial memory and plasticity at inputs to distal dendrites of CA1 pyramidal neurons. *Cell* **119**, 719–732.

Pape HC (1996). Queer current and pacemaker: the hyperpolarization-activated cation current in neurons. *Annu Rev Physiol* **58**, 299–327.

Paxinos G & Watson C (1998). *The Rat Brain in Stereotaxic Coordinates*, 4th edn. Academic Press, London.

Pinault D (2003). Cellular interactions in the rat somatosensory thalamocortical system during normal and epileptic 5–9 Hz oscillations. *J Physiol* **552**, 881–905.

Pinault D (2005). A new stabilizing craniotomy-duratomy technique for single-cell anatomo-electrophysiological exploration of living intact brain networks. *J Neurosci Meth* **141**, 231–242.

Pinault D, Leresche N, Charpier S, Deniau JM, Marescaux C, Vergnes M & Crunelli V (1998). Intracellular recordings in thalamic neurones during spontaneous spike and wave discharges in rats with absence epilepsy. *J Physiol* **509**, 449–456.

Poolos NP (2004). The yin and yang of the H-channel and its role in epilepsy. *Epilepsy Curr* **4**, 3–6.

Renier WO & Coenen AML (2000). Human absence epilepsy: the WAG/Rij rat as a model. *Neurosci Res Com* **26**, 181–191.

Robinson RB & Siegelbaum SA (2003). Hyperpolarization-activated cation currents: from molecules to physiological function. *Annu Rev Physiol* **65**, 453–480.

Rudolf G, Bihoreau MT, Godfrey RF, Wilder SP, Cox RD, Lathrop M, Marescaux C & Gauguier D (2004). Polygenic control of idiopathic generalized epilepsy phenotypes in the genetic absence rats from Strasbourg (GAERS). *Epilepsia* **45**, 301–308.

Santoro B & Baram TZ (2003). The multiple personalities of h-channels. *Trends Neurosci* **26**, 550–554.

Santoro B, Wainger BJ & Siegelbaum SA (2004). Regulation of HCN channel surface expression by a novel C-terminal protein–protein interaction. *J Neurosci* **24**, 10750–10762.

Seidenbecher T, Staak R & Pape HC (1998). Relations between cortical and thalamic cellular activities during absence seizures in rats. *Eur J Neurosci* **10**, 1103–1112.

Seifert R, Scholten A, Gauss R, Mincheva A, Lichter P & Kaupp UB (1999). Molecular characterization of a slowly gating human hyperpolarization-activated channel predominantly expressed in thalamus, heart, and testis. *Proc Natl Acad Sci U S A* **96**, 9391–9396.

Shah MM, Anderson AE, Leung V, Lin X & Johnston D (2004). Seizure-induced plasticity of h channels in entorhinal cortical layer III pyramidal neurons. *Neuron* **44**, 495–508.

Slaght SJ, Leresche N, Deniau JM, Crunelli V & Charpier S (2002). Activity of thalamic reticular neurons during spontaneous genetically determined spike and wave discharges. *J Neurosci* **22**, 2323–2334.

Song I, Kim D, Choi S, Sun M, Kim Y & Shin HS (2004). Role of the α1G T-type calcium channel in spontaneous absence seizures in mutant mice. *J Neurosci* **24**, 5249–5257.

Strauss U, Kole MHP, Bräuer AU, Pahnke J, Bajorat R, Rolfs A, Nitsch R & Deisz RA (2004). An impaired neocortical I_h is associated with enhanced excitability and absence epilepsy. *Eur J Neurosci* **19**, 3048–3058.

Stuart GJ & Williams SR (2000). Co-localization of I_H and I_T channels in dendrites of thalamocortical neurons. *Soc Neurosci Abstract* **30**, 610.19.

Su H, Sochivko D, Becker A, Chen J, Jiang Y, Yaari Y & Beck H (2002). Upregulation of a T-type Ca^{2+} channel causes a long-lasting modification of neuronal firing mode after status epilepticus. *J Neurosci* **22**, 3645–3655.

Talley EM, Solórzano G, Depaulis A, Perez-Reyes E & Bayliss DA (2000). Low-voltage-activated calcium channel subunit expression in a genetic model of absence epilepsy in the rat. *Mol Brain Res* **75**, 159–165.

Tsakiridou E, Bertollini L, de Curtis M, Avanzini G & Pape HC (1995). Selective increase in T-type calcium conductance of reticular thalamic neurons in a rat model of absence epilepsy. *J Neurosci* **15**, 3110–3117.

van Welie I, van Hooft JA & Wadman WJ (2004). Homeostatic scaling of neuronal excitability by synaptic modulation of somatic hyperpolarization-activated I_h channels. *Proc Natl Acad Sci* **101**, 5123–5128.

Vasilyev DV & Barish ME (2004). Regulation of the hyperpolarization-activated cationic current I_h in mouse hippocampal pyramidal neurones by vitronectin, a component of extracellular matrix. *J Physiol* **560**, 659–675.

Vergnes M, Marescaux C & Depaulis A (1990). Mapping of spontaneous spike and wave discharges in Wistar rats with genetic generalized non-convulsive epilepsy. *Brain Res* **523**, 87–91.

Vincent P & Brusciano D (2001). Cyclic AMP imaging in neurones in brain slice preparations. *J Neurosci Meth* **108**, 189–198.

Wang J, Chen S, Nolan MF & Siegelbaum SA (2002). Activity-dependent regulation of HCN pacemaker channels by cyclic AMP: signaling through dynamic allosteric coupling. *Neuron* **36**, 451–461.

Waxman SG (2001). Transcriptional channelopathies: an emerging class of disorders. *Nat Rev Neurosci* **2**, 652–659.

Yu H, Wu J, Potapova I, Wymore RT, Holmes B, Zuckerman J, Pan Z, Wang H, Shi W, Robinson RB, El-Maghrabi MR, Benjamin W, Dixon J, McKinnon D, Cohen IS & Wymore R (2001). MinK-related peptide 1: a β subunit for the HCN ion channel subunit family enhances expression and speeds activation. *Circ Res* **88**, 84–87.

Zhang Y, Mori M, Burgess DL & Noebels JL (2002). Mutations in high-voltage-activated calcium channel genes stimulate low-voltage-activated currents in mouse thalamic relay neurons. *J Neurosci* **22**, 6362–6371.

Zhang Y, Vilaythong AP, Yoshor D & Noebels JL (2004). Elevated thalamic low-voltage-activated currents precede the onset of absence epilepsy in the SNAP25-deficient mouse mutant coloboma. *J Neurosci* **24**, 5239–5248.

Acknowledgements

We thank Any Boehrer for the breeding and selection of GAERS, Dr Pascale Piguet and Stéphanie Klipfel from Neurex for support with animal transport, and Estelle Koning for excellent technical support. Prof. Dr U. Gerber, University of Zürich, and members of the Lüthi lab are greatly acknowledged for constructive comments on the manuscript. A.L. is supported by the Swiss National Science Foundation (No. 3100A0-103655), the Jubiläumsstiftung der Schweiz. Mobiliarversicherungsgesellschaft and the Fonds zur Förderung von Lehre und Forschung. T.Z.B. and A.L.B. are supported by NIH NS35439 research grant, and A.L.B. also by an NIH pre-doctoral grant NS47993. D.P. is supported by the French Institute of Health and Medical Research (INSERM) and by the University of Louis Pasteur, the Fondation française pour la recherche sur l'épilepsie, and the Electricité de France.